PAPER

Gold nanoparticle shape dependence of colloidal stability domains†

Antonio Carone, Samuel Emilsson, Pablo Mariani, Anthony Désert [ID] *
and Stephane Parola [ID]

Controlling the spatial arrangement of plasmonic nanoparticles is of particular interest to utilize inter-particle plasmonic coupling, which allows changing their optical properties. For bottom-up approaches, colloidal nanoparticles are interesting building blocks to generate more complex structures *via* controlled self-assembly using the destabilization of colloidal particles. For plasmonic noble metal nanoparticles, cationic surfactants, such as CTAB, are widely used in synthesis, both as shaping and stabilizing agents. In such a context, understanding and predicting the colloidal stability of a system solely composed of AuNPs and CTAB is fundamentally crucial. Here, we tried to rationalize the particle behavior by reporting the stability diagrams of colloidal gold nanostructures taking into account parameters such as the size, shape, and CTAB/AuNP concentration. We found that the overall stability was dependent on the shape of the nanoparticles, with the presence of sharp tips being the source of instability. For all morphologies evaluated here, a metastable area was systematically observed, in which the system aggregated in a controlled way while maintaining the colloidal stability. Combining different strategies with the help of transmission electron microscopy, the behavior of the system in the different zones of the diagrams was addressed. Finally, by controlling the experimental conditions with the previously obtained diagrams, we were able to obtain linear structures with a rather good control over the number of particles participating in the assembly while maintaining good colloidal stability.

Introduction

One peculiarity of colloidal nanoparticles (NPs) is the possibility to use them as discrete entities or as building blocks to form hierarchical structures with new and different properties. Controlling the formation of discrete clusters of NPs to obtain very large 2D and 3D assemblies or even crystals composed of many nanoparticles is one of the most exciting challenges in the nanomaterial chemistry.[1,2] For noble metal nanoparticles, this is especially true because of the interesting change in the plasmonic resonance arising from the collective effects.[3] However, in order to obtain a material with desired properties, predicting and tuning the colloidal stability of NPs is a fundamental prerequisite.

For lyophobic metal nanoparticles, the colloid can remain as individual particles only if some mechanism can counter the attractive van der Waals forces occurring between the NPs.[4] Surface functionalization is a common way to obtain a stable colloid, providing electrostatic, steric, or electrosteric

stabilization.[5] Electrostatic stabilization is based on Coulomb repulsion between particles having the same surface charge sign, preventing the particles from coming into close contact where the attractive short-distance van der Waals forces dominate. Similarly, for steric stabilization, the contact is avoided by adsorbing bulky molecules on the surface, which act as a spacer to prevent particle aggregation. Finally, electrosteric stabilization can be seen as a combination of both.[6,7]

Through the application of these mechanisms, noble metal NPs made of gold or silver, as well as other systems such as quantum dots or titanium oxide colloids can be made stable for months without any noticeable sign of aggregation.[8,9] For gold nanoparticles (AuNPs), thiols,[10–12] polyelectrolytes,[13–16] surfactants,[17] and citrates,[18–20] are some of the main coating agents used to maintain the colloidal stability. Among these, cationic surfactants, such as hexadecyltrimethylammonium bromide (CTAB), can also play an important role as shaping agents in the synthesis of anisotropic AuNPs, such as gold nanorods (AuNRs) and gold bipyramids (AuBPs).[21–23] Nikoobakht and El-Sayed proposed that CTAB could form a bilayer structure around the gold surface.[24] This idea was later supported by Murphy *et al.* and is nowadays widely accepted.[25–27] The first CTAB layer binds with the gold surface *via* electrostatic interaction between the cationic quaternary ammonium and the anionic bromide gold complexes. The second layer interacts with the first layer

through the entangling of alkyl chains and exposing the cationic ammonium group outwards.[26] The bilayer configuration of CTAB on the AuNPs was found to be in a dynamic equilibrium with the free CTAB in solution.[28,29] Based on Raman measurements, Lee *et al.* showed that reducing CTAB concentration in solution leads to the collapse of the ordered structure, thus reducing the colloidal stabilization efficiency of the double layer.[29] However the exact concentration of CTAB above which the system is stable is difficult to determine because other parameters also play a role. As already pointed out by Kotov and collaborators, to predict the colloidal stability of nanoparticles, parameters such as the shape of the particles and ligand coverage must be taken into consideration.[30] Indeed, a study of the impact of these parameters on the colloidal stability appears crucial in order to achieve good control in the self-assembly process.[31] To the best of our knowledge, no systematic study has yet been performed on colloidal stability *versus* the shape or size in the case of AuNPs.

We propose a complete investigation that would make a contribution regarding insights on controlling the colloidal stability of surfactant-stabilized AuNPs. Taking advantage of our previous works[32,33] on the synthesis of pentatwinned AuNPs with a fine control of their shape, size, and plasmonic properties, we evaluated the colloidal stability of CTAB-stabilized AuNPs. The use of a common synthetic method allows obtaining particles with a comparable surface state (same surfactant, eventual impurities, reactants). Different stability diagrams were obtained with the help of UV-vis-NIR spectroscopy to evaluate the importance of the size, shape, and ratio between the AuNPs and CTAB concentrations. Lastly, the assembled NPs were studied by transmission electron microscopy (TEM) employing three different methods to retrieve the size distribution of the aggregates in suspension. This allowed also to understand the different ways NPs assemble as a function of the CTAB concentration.

Results and discussion

Nanoparticles preparation and characterization

Different shapes and sizes of CTAB-stabilized pentatwinned gold nanoparticles were synthesized to study their colloidal stability when the surfactant concentration was reduced. The protocol used to produce the AuNPs was a seed-mediated growth method, recently developed by our group, which allowed us to obtain different morphologies in a concentrated

manner.[32] Having nearly monodisperse nanoparticles with a high shape purity (above 95%) was crucial to obtain consistent results. A total of six different batches of gold nanobipyramids (AuBPs), gold nanospheres (AuNSs), gold nanorods (AuNRs), and gold nanoellipsoids (AuNEs) were produced (Fig. S1†). The dimensions of the NPs for each batch, obtained through statistical analysis over 300 NPs through transmission electron microscopy (TEM), as well as the position of the localized surface plasmon resonance (LSPR) bands measured by UV-vis-NIR spectroscopy are listed in Table 1. Similarly to what has been reported in the literature, the combination of inductively coupled plasma (ICP) with UV-vis-NIR spectroscopy allowed us to determine experimentally the molar extinction coefficient at 400 nm for the different morphologies (Table S1†).[34,35] The volume and surface of s single particle for the different shapes were calculated starting from the obtained TEM statistics (Fig. S2 and Table S2†).

Nanoparticles stability

When the CTAB concentration ([CTAB]) was diminished under a critical value, for the morphologies taken into account in this study, several changes in the spectrum indicated a reorganization of the system through aggregation of a single NP (Fig. 1).[36,37]

For AuBP-83, when [CTAB] was reduced to 0.01 mM, after 1 h, the L-LSPR centered at 762 nm was reduced in intensity and a broad band from 800 to 1100 nm appeared (Fig. 1a). The kinetic of the aggregation was found to be dependent on the CTAB concentration (Fig. 1b). The reduction of [CTAB] to 0.03 mM led to a 5% reduction in the intensity of the L-LSPR at 762 nm after 24 h (Fig. 1b). Reducing [CTAB] below 0.03 mM led the spectra to show a significant reduction in the L-LSPR intensity already in the first 10 min. At 0.01 mM of [CTAB], the L-LSPR was diminished by around 60% after 10 min. For AuNS-45, the isotropic objects generated a single plasmonic band centered at 530 nm (Fig. 1c). When [CTAB] was reduced to 0.00125 mM, after 1 h, the intensity of the main band was reduced and a new broad band centered at 840 nm appeared. In the case of AuNE-18 (Fig. 1d), the objects were slightly anisotropic (A.R. = 1.4), so the spectrum presented a band between 450 and 650 nm with two peaks at 524 and 568 nm, attributed to the T-LSPR and the L-LSPR, respectively. When [CTAB] was reduced to 0.005 mM, after 1 h, the intensity of the T-LSPR was reduced while the L-LSPR was shifted to 708 nm. In a similar

Table 1 Characterization results of the different AuNPs morphologies. For the TEM measurements, the error is expressed by standard deviation

Sample name	Length (nm)	Width (nm)	A.R.	T-LSPR[a] (nm)	L-LSPR (nm)
AuNS-24	24 ± 2	—	—	523	—
AuNS-45	45 ± 2	—	—	530	—
AuBP-83	83 ± 6	26 ± 2	3.2	512	762
AuBP-147	147 ± 9	36 ± 3	4.1	513	927
AuNE-18	18 ± 4	13 ± 2	1.4	524	568
AuNR-65	65 ± 5	26 ± 2	2.5	520	694

[a] LSPR for AuNS samples.
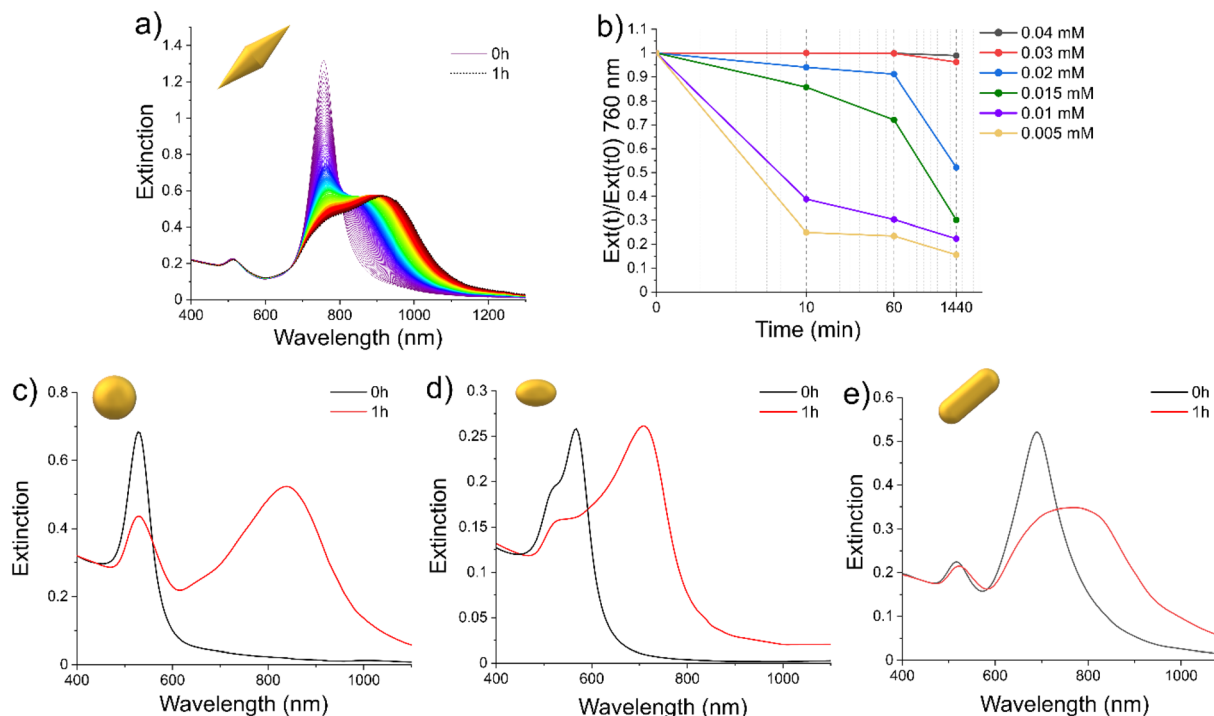
Fig. 1 Effects of [CTAB] reduction on the optical response. (a) Superposition of different spectra of AuBP-83 taken every 10 s when [CTAB] was reduced to 0.01 mM. (b) Intensity reduction kinetic of the L–LSPR of AuBP-83 at different CTAB concentrations. Spectral changes after 1 h of (c) AuNS-45 at 0.00125 mM CTAB, (d) AuNE-18 at 0.005 mM CTAB, and (e) AuNR-65 0.005 mM CTAB.

way, for AuNR-65 when [CTAB] was reduced to 0.005 mM, the L-LSPR centered at 694 nm was red-shifted to 776 nm and broadened (Fig. 1e). It was interesting to note that the aggregation was not reversible. The addition of CTAB at any time resulted in a freezing of the aggregation process but not a return to the initial configuration (Fig. S3†).

The changes in the spectra were coherent with aggregation of the plasmonic objects due to the [CTAB] reduction. However, the difference in [CTAB] required to destabilize the systems between AuNSs and AuBPs (0.00125 and 0.01 mM, respectively) suggested that other parameters can also have an impact on the colloidal stability. In order to explore this hypothesis, we proceeded to extensively study the colloidal stability, testing the impact of the morphology as well as different [NPs]/[CTAB] ratios. Several stability diagrams, one for each morphology, were obtained and are presented in Fig. 2.

For convenience, in the diagrams, the [NPs] were converted for specific Au^0 surfaces (the diagrams expressed in [NPs] can be found in Fig. S4†). The detailed procedure to build the diagrams is described in the methods section. In the diagrams, the gamma domain (green points) refers to a condition where the colloid was found to be stable. This means that no change in the plasmon resonance was observed in the 24 h after preparation (Fig. S5a†). The beta domain (yellow points) refers to a condition where the particles were found to be metastable: the spectrum showed signs of aggregation (red-shift/shouldering), but no decrease in the extinction at 400 nm was observed (Fig. S5b†). The alpha domain (red points) refers to an area where the colloid was found to be unstable. Along with the signs

of aggregation (appearance of a new band/shouldering) 24 h after preparation, the intensity at 400 nm was found to decrease, as well as the overall intensity of the spectrum, indicating a precipitation process (Fig. S5c†). The samples in this area usually showed a clear supernatant with a sediment of NPs at the bottom of the cuvette.

For bipyramids, two different sizes were tested: AuBP-83 and AuBP-147 (Fig. 2). For both AuBPs sizes, the particles were stable when free [CTAB] was above 0.032 mM. The metastability area was found to space from 0.032 mM to 0.013 mM CTAB, while the sample was unstable for values below 0.013 mM CTAB. For AuNR-65 the metastability area was comprised between 0.0175 and 0.0075 mM CTAB, while the instability area started below 0.0075 mM CTAB. For AuNE-65, the metastability was reached when [CTAB] was between 0.01 mM to 3 μM, while the instability area reached below 3 μM.

Finally, spheres were found to be much more stable compared to other shapes. For nanospheres, two different sizes were tested: AuNS-45 and AuNS-24. For both AuNSs sizes, the metastability area was between 4 and 2 μM while the instability area started for values below 2 μM. From the analysis of the diagrams, it could be noted that two batches of particles having the same shape, but different sizes, shared the same stability trend. This was the case both for isotropic particles, like AuNSs, and also for anisotropic ones, like AuBPs (Fig. 2). This could suggest that, for this order of magnitude, the size of the particles do not have an impact on their stability. Moreover, varying the Au^0 total surface for the range taken in the examination did not play a role in the stability. To better understand this
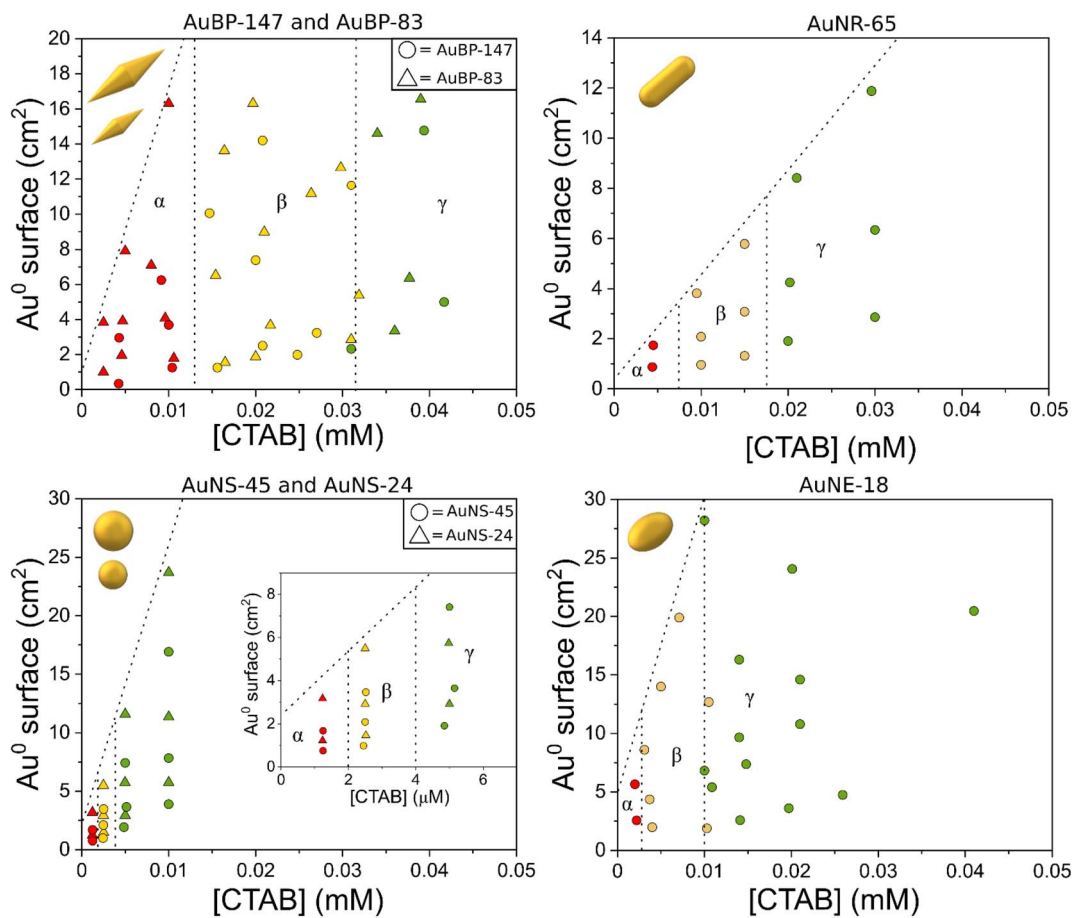
Fig. 2 Stability diagrams of the different AuNPs. The red points indicate that the system was found to be unstable, the yellow points a metastable condition, and the green points a stable condition.

evidence, it was possible to estimate the amount of CTAB originally adsorbed on the surface of the particles using a coverage value of 0.8 molecules per nm^2 for CTAB.[38] The number of CTAB molecules on the surface of the NPs was found to be one to three orders of magnitude inferior to the free CTAB in solution (Fig. S4†). It is possible to imagine that changing the total surface did not have a significant impact on the equilibrium between the free CTAB and adsorbed CTAB on the particles. This effect may not be valid if the specific Au^0 surface is increased far above the value in this study ($28.2 \ cm^2$). However, increasing the Au^0 surface above this value while maintaining the same setup could be challenging from an experimental point of view. Despite this, the lack of influence of the size and surface on the stability allowed us to safely investigate the effect of the shape.

From the stability diagrams, it was possible to note that the shape plays the major role in the overall colloidal stability. The CTAB concentration needed to maintain the system stable was observed to increase with the anisotropy of the particles. In a similar trend, the extension area of the metastability zone (yellow points in Fig. 2) was progressively smaller when the anisotropy was reduced. Also in the zeta potential measurements, the effect of the shape on the stability was visible (Fig. 3). The colors of the points in Fig. 3 are linked with the results

obtained in the stability diagrams (Fig. 2): the green points indicate that the system was stable, while the yellow points show the system aggregated. It is possible to note that for AuBPs, values above +30 mV were present at 0.04 mM CTAB, while for spheres, a value above +30 mV was present at 0.004 mM CTAB. Particles having a zeta potential value above +30 mV (or below −30 mV) are commonly considered stable. The zeta potential measurements were in agreement with the stability diagrams for all the different shapes, showing potentials above +30 mV when [CTAB] was increased to values within the stability area. Even if stability was found to be dependent on the anisotropy, the aspect ratio itself was found to not be indicative of the stability. AuBP-83 and AuBP-147 shared the same stability diagram but had a different aspect ratio (3.2 and 4.1, respectively, Table 1). The effect of the shape on the stability trend could be better explained by considering the reduced effectiveness of CTAB to stabilize the tips at different curvatures. It is known that for anisotropic NPs, like AuBPs and AuNRs, the CTAB double-layer density on the tips is reduced because of the curved geometry that prevents the effective stacking of the hydrophobic chains of the surfactant.[38,39] TEM images of the tips of AuBP-83 and AuBP-147 showed that for both the size of the tips radius was almost identical, with a radii of 9 ± 1 and 9.5 ± 0.8, respectively, explaining why even despite
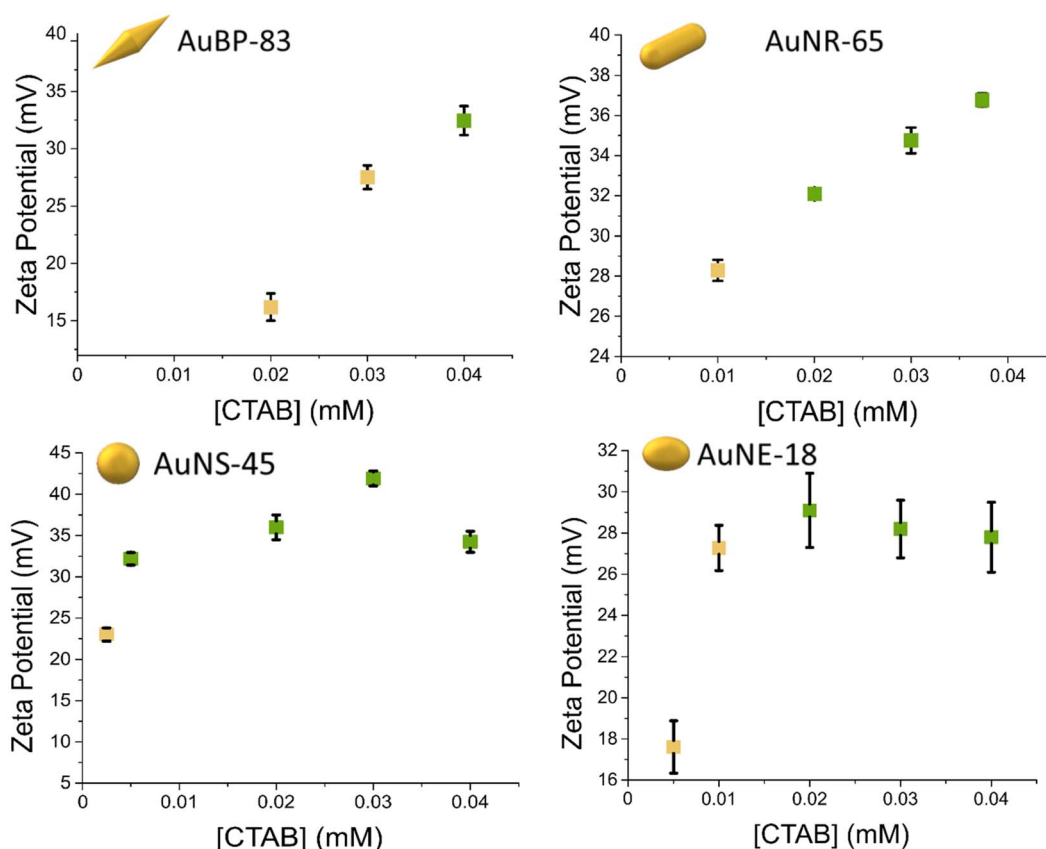
Fig. 3 Zeta potential measurements at different CTAB concentrations. UV-vis–NIR measurements indicated that the green points were stable after 24 h, while the yellow points were found to aggregate.

having a different A.R. the NPs share the same stability diagram. For AuBPs, it is possible to imagine that the tips were already exposed at 0.03 mM CTAB when bringing the system to assembly. The different reactivity of the sharp tips could also explain the difference in the extension of the beta zone, being widely extended for AuBPs, while gradually diminishing for AuNRs and AuNEs, and almost absent for AuNSs.

To further explore the way the systems reorganize when [CTAB] was reduced, the samples were characterized by TEM. To avoid any possible change in the nature of the aggregates upon sample drying on the TEM grid, the colloidal aggregates were previously encapsulated in a silicate shell. The TEM images confirmed that reducing the CTAB concentration led to the system aggregating (Fig. 4). The absence of any other ligand than CTAB allowed us to exclude any other ligand/linker contribution and permitted us to attribute the assembly to a pure electrostatic mechanism. When [CTAB] was reduced, the number of charges on the surface of the particles diminished as well (Fig. 3), to a point where the attractive van der Waals force became predominant over the repulsive one. The driving force of the assembly being a partial deficiency of CTAB was coherent with the absence of spacing between two nanoparticles in the aggregate, as could be observed in the TEM images (Fig. 4). For comparison, a solution of AuBPs in the stability zone, deposited on a TEM grid, showed no contact between the tips of the particles, even in close

packed condition (Fig. S6†). Instead of having an uncontrolled aggregation, when the system was in the metastable zone, the formation of linear chains was observed for all morphologies. The formation of nanospheres linear chains has been established to be caused by the different repulsions (i.e., activation energy) that a nanoparticle must overcome before attaching to the end of a chain or on its sides.[40] A nanosphere approaching the end of the chain experiences repulsion similar to a sphere-to-sphere collision, whereas an approach from the side of the chain leads to a stronger repulsion similar to a sphere-to-rod situation.[41] In a similar way, the formation of chains for anisotropic NPs in acetonitrile medium was also found by Kar *et al.* to be driven by the surface charge of the NPs.[42] In the same study, it was highlighted that the formation of a linear assembly could be observed when the zeta potential was in the range between 10 and 20 mV. Similar to the study of Kar *et al.*, zeta potential measurements of our system showed a potential between 15 and 30 mV when the systems were brought to the metastability zone (Fig. 3).

Moreover, for the anisotropic shapes a tip-to-tip contact between the NPs was observed, supporting the idea that the tips of the anisotropic structure were activated when [CTAB] was diminished (Fig. 4).

To further explore this evidence, the impact of the [CTAB] on the type of contact for AuBP-83 was investigated. When the system was in the center of the metastable zone (Fig. 2), at
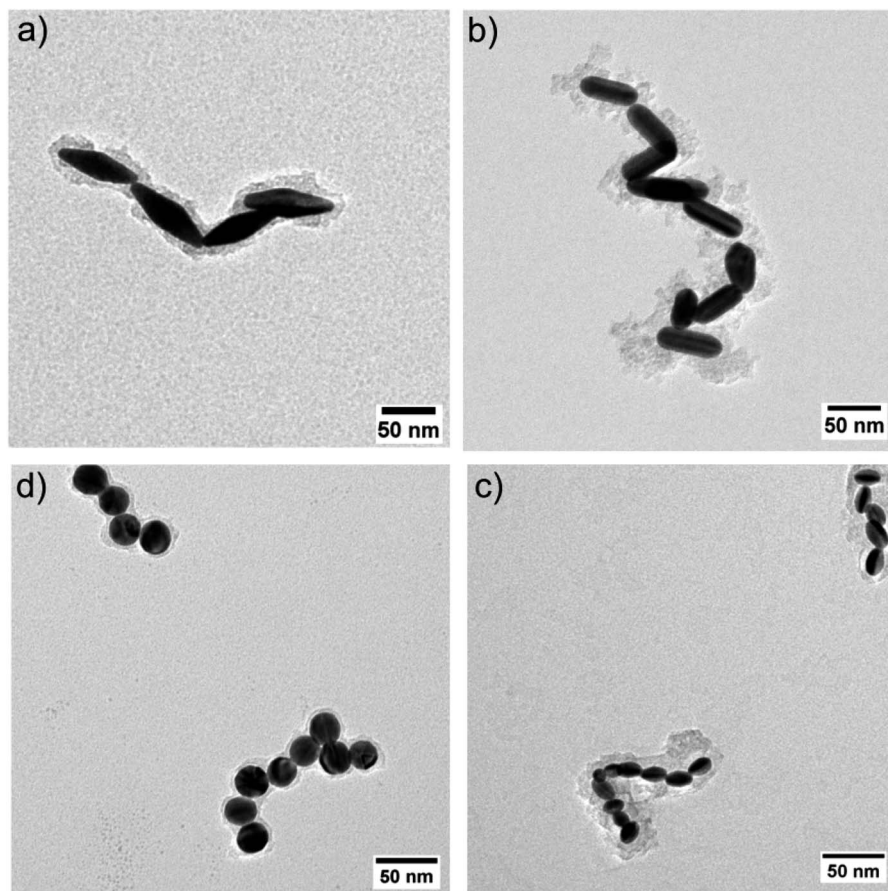
Fig. 4 TEM images of AuNPs covered with silicate: (a) AuBP-83, 0.02 mM CTAB, (b) AuNR-65 0.01 mM CTAB, (c) AuNE-18, 0.003 mM CTAB, and (d) AuNS-24, 0.002 mM CTAB.

0.02 mM CTAB, linear chains were observed (Fig. 5a and b). Statistical analysis of over 400 NPs showed a predominance of the tip-to-tip contact (around 67%). When the system was in the center of the instability zone at 0.005 mM CTAB, an anarchic aggregation was observed. Statistical analysis showed that the tip-to-tip contact was no longer favored (Fig. 5a and c). An increased quantity of different types of contact (like side-to-side) was also confirmed by UV-vis-NIR spectroscopy, where a red-shift of the T-LSPR was present in the spectrum, along with the red-shift of the L-LSPR (Fig. 5d).[43] For the AuBPs objects it was then possible to distinguish two different situations: (i) when the system was in the metastable zone, the tips of the AuBPs did not have sufficient CTAB adsorbed to prevent aggregation, inducing assembly with a tip-to-tip contact and (ii) when the system was in the unstable zone, the entire surface of the particles was no longer sufficiently stabilized and the system aggregated with no preferential orientation as big aggregates composed of many NPs. It was important to note, however, that the separation line between the two domains was a soft border since the change in reactivity was gradual from one zone to the other.

Encapsulating the AuNPs with silicate allowed determining the relative number of particles participating in the different types of aggregates (dimers, trimers, etc.). A comparison of the distribution of the assembly type evaluated with different methodologies is presented in Fig. 6a. Statistical analysis obtained with the silicate method (light-gray bars) for AuNEs at 0.005 mM CTAB showed that the system was mostly composed of dimers (Fig. 6a and S7†). This result was in line with cryo-TEM measurements (blue bars) indicating that silicate treatment was effective in preventing any possible change in the nature of the aggregate upon sample drying (Fig. S8†). The dark-gray bars indicate a complementary method that was tested for the formation of Au@Ag core–shell structures for the same purpose (Fig. 6b and S9†), similarly to what was done in a work of Li et al.[44] Also the silver method was in line with the silicate and cryo-TEM measurements. However, the Au@Ag method suffered from poor adaptability when applied for other shapes than AuNEs. This was probably due to the change in reactivity of Au surfaces when changing the shape of AuNPs. For this reason, the Au@Ag method was abandoned for the silicate method, which could provide excellent adaptability with different systems.

However, changing the [CTAB] resulted in a variation of the length distribution of the chains formed. For AuBP-83, the type of aggregates frequency when [CTAB] was varied in the meta-stability zone are presented in Fig. 6c. When the sample was prepared at 0.02 mM CTAB and incubated for 1 h, mostly dimers were formed (Fig. S10†). Instead, when [CTAB] was set at
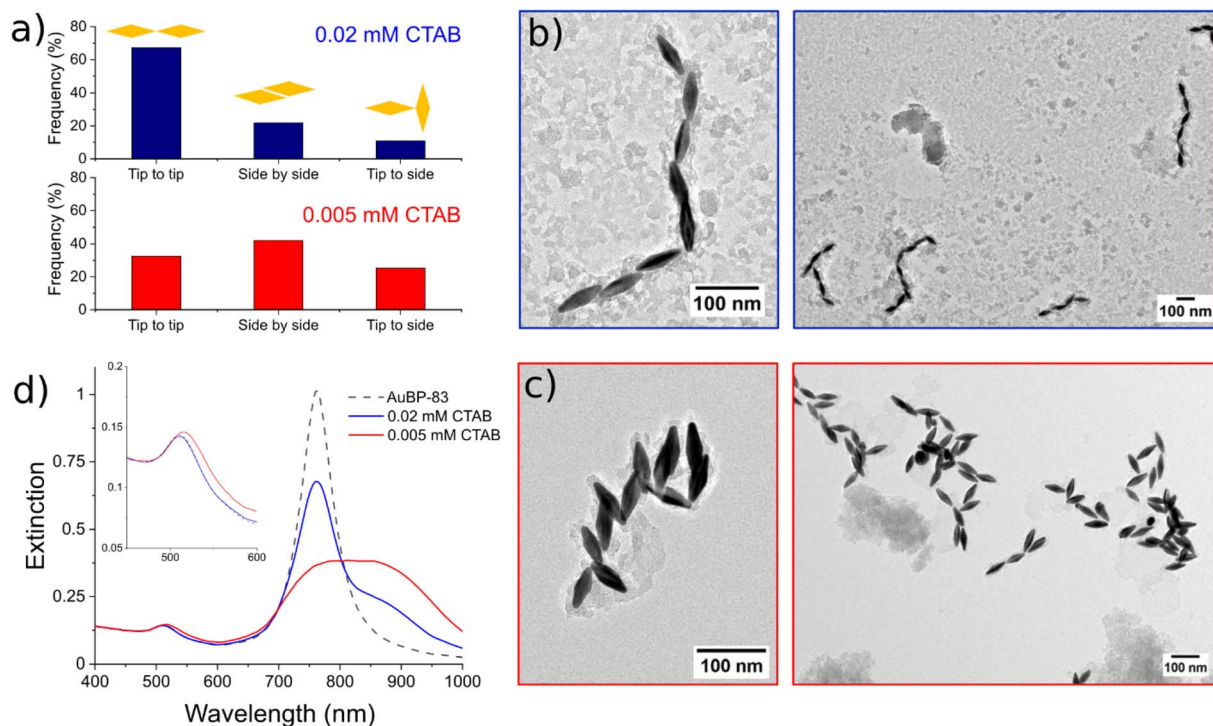
Fig. 5 (a) Statistics of the type of contact distribution at different CTAB concentration. TEM images of AuBP-83 at 0.02 mM CTAB (b) and 0.005 mM CTAB (c). (d) Superposition of the spectra of the assemblies made at different CTAB concentrations. In the inset, the spectral range between 450 and 600 nm is enlarged to better visualize the change in the T-LSPR.
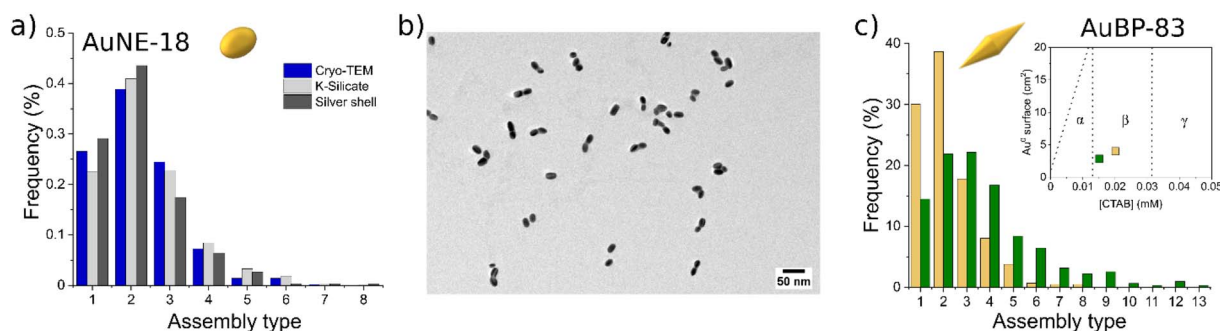

Fig. 6 (a) Statistics of the number of particles participating in the assemblies measured by TEM with three different strategies. (b) TEM images of the AuNE-18 aggregates coated with the silver shell. (c) Statistics of the number of particles participating in the assemblies for AuBP-83 measured by TEM at different CTAB concentrations. The inset clarifies the position of the system with respect to the diagram in Fig. 2.

0.015 mM for 1 h, the reduction of the number of monomers and dimers in spite of the formation of longer chains was observed (Fig. S11†). The time after preparation also had an effect on the length of the chains, with samples in the same zone of the diagram having different chain lengths according to when the aggregation process was stopped by the addition of CTAB (Fig. S12†).

Conclusions

The colloidal stability of CTAB-capped AuNPs was studied and several stability diagrams evaluating the impact of the ratio of [NPs]/[CTAB], and shapes and sizes of the NPs were proposed.

Comparisons of the different diagrams showed a clear correlation between the colloidal stability and the shape of the nanoparticles. It was found that the more stable gold nanospheres could maintain the colloidal stability even when the surfactant concentration in the solution was 0.005 mM, while the anisotropic AuBPs were found to be unstable at 0.03 mM CTAB. This was caused by the presence of tips with high curvature in the case of anisotropic nanoparticles, where the ability of CTAB to be densely packed is strongly reduced. Conversely, changing the size of the NPs or their concentration had no impact on the overall stability, at least in the range taken into consideration in our work. Moreover, a metastable zone was found for all the investigated morphologies, where

the system was found to aggregate in a controlled way while maintaining the colloidal stability. TEM microscopy combined with silicate encapsulation allowed the observation of discrete linear aggregates of NPs representative of the colloidal state, which were formed when the system was in these metastable conditions. The formation of linear chains, in this case made in the absence of other ligands, confirmed the hypothesized electrostatic driving force behind the formation of these linear structures. Moreover, the way in which the AuBPs came into contact in the aggregate organization was also found to be dependent on the CTAB concentration with a preferential tip-to-tip assembly when the system was in the metastable zone, against the anarchic aggregation observed when the system was in the unstable zone. Achieving control over the type of assembly by precise adjustment of the surfactant concentration, combined with the possibility to freeze and stabilize the system at any time, allowed us to obtain a controlled self-assembly process in the absence of any other linker/ligand than CTAB. We believe these results will be useful in controlling and rationalizing the colloidal stability of AuNPs as well as providing a way to arrange them in more complex structures for further exploration of the properties of finite aggregates and for use in optics, catalysis, electronics, or other fields of applications.

Materials and methods

Tetrachloroauric acid trihydrate (HAuCl$_4$·3H$_2$O, 99.9%), silver nitrate (AgNO$_3$, 99.99%), resorcinol (99%), N,N,N',N'-tetramethylguanidine (99%), and potassium silicate (SiO$_2$: K$_2$O 2.5 : 1 wt%, anhydrous) were purchased from Alfa Aesar. BDAC (benzylhexadecyldimethylam-monium chloride, 97%), hexadecyltrimethylammonium bromide (CTAB, 99%, ref. H6269-250G), 8-hydroxyquinoline (99%), sodium borohydride (NaBH$_4$, 98%), L-ascorbic acid (99%), eriochrome black T, and catechol (98%) were purchased from Sigma-Aldrich. Citric acid monohydrate (99.5%) was purchased from Merck. Powder hexadecyltrimethylammonium chloride (CTAC, 99%) was purchased from Acros Organics. Cellulose tubular membranes (12 kDa) were purchased from Spectra-Por. Milli-Q water with a resistivity above 18.2 MΩ cm was used in all the experiments.

AuNPs synthesis and purification

Pentatwinned AuNPs were obtained using a seed-mediated growth method fully described in our previous work.[32] Different morphologies and sizes were obtained in a concentrated manner ([Au^0] = 15 mM). To avoid any aggregation during the purification, the particles were centrifuged at no more than 8000 rpm for 10 min and always redispersed in 5 mM CTAB. Subsequently, the particles were purified by dialysis using a solution at 0.5 mM CTAB. The dialysis served to increase the ratio of [Au^0]/[CTAB] by setting the CTAB concentration to 0.5 mM in a soft way while keeping invariant the Au^0 concentration. The final CTAB concentration was titrated by a spectrophotometric method (Fig. S13†).[45] The [Au^0] was determined

by recording the extinction at 400 nm (Table S1†).[35] The se prepared suspensions were stable for months.

Construction of the stability diagrams

To probe the stability of the AuNPs at given gold and surfactant concentrations, we proceeded by diluting a concentrated stock solution with a known [Au^0] and [CTAB] ratio. Different stock suspensions were prepared with different [Au^0]/[CTAB] ratios, allowing us to cover a wide range of points (for convenience [CTAB] was fixed at 0.5 mM for all the stock suspensions). In a typical experiment, a variable amount (a few tens of microliters) of a concentrated stock AuNPs solution (0.5 mM CTAB) was pipetted in a cuvette, followed by Milli-Q water to reach a final volume of 1 mL. After mixing, the stability of the suspension was monitored by UV-vis-NIR spectrometry at 10 min, 1 h, and 24 h. It is important to note that inversing the order of mixing did not influence the general trend but led to poor reproducibility for points on the border of the stability/instability zones. Also, using CTAB from a different supplier did not have a relevant impact. The produced diagrams were both expressed in Au^0 surface (Fig. 2) and the number of particles (Fig. S4†). The Au^0 surface was calculated by multiplying the surface of one particle by the number of particles (Table S2 and Fig. S4†). The aggregation process could be frozen by increasing the concentration of CTAB to 1 mM.

Silicate encapsulation for TEM imaging

In order to encapsulate the system in a silicate shell, 1 mL of the stabilized suspension (typically [Au^0] = 0.3 mM and [CTAB] = 1 mM) was introduced under stirring (500–600 rpm) into 1 mL of an aqueous solution of potassium silicate (3 wt%) previously heated at 60 °C in a water bath. The mixture was kept at 60 °C for 1–2 minutes and then allowed to cool slowly to room temperature (RT). After 1 h at RT, the particles were washed with water three times by successive centrifugation (5 min, 10 000 rpm). The final dispersion was made in 0.5 mL of water using a sonic bath. It was observed that changing the initial [Au^0] did not require any adjustment of the protocol. Instead, when the CTAB concentration was above 1 mM, individual silicate particles were present along with the target core–shell structures. In order to perform TEM analysis, a few microliters of this suspension was then deposited into a carbon-coated copper grid and left to dry.

AuNE-18@Ag for TEM imaging

In order to encapsulate the system in a silver shell, 5 μL of 5 mM AgNO$_3$ and 100 μL of 20 mM of ascorbic acid were introduced into 1 mL of the stabilized AuNEs suspension (typically [Au^0] = 0.3 mM and [CTAC] = 30 mM). The mixture was homogenized by manual mixing and placed in a water bath at 85 °C for 30 min. The color changed from blue to pink (Fig. S14†). The particles were then washed twice with 1 mM CTAC by successive centrifugation (10 min, 10 000 rpm) and redispersed in 1 mL of 1 mM CTAC.

Characterization

UV-vis-NIR spectra were recorded with a PerkinElmer UV-vis-NIR Lambda 750 spectrometer using disposable PMMA plastic cuvettes. TEM images were acquired using a JEOL 2100F equipped with a Gatan ultrascan 1000 camera operating at 200 kV. Cryo-TEM images were acquired using a Philips CM120 system equipped with a cryo-holder Gatan 626 and Gatan Orius camera. Zeta potential measurements were performed using an Anton Paar litesizer 500 and a Malvern zetasizer nano ZS instruments.

Author contributions

Conceptualization, A. C., A. D. and S. P.; investigation, A. C., S. E. and P. M.; funding acquisition, A. D. The manuscript was written through contributions of all authors. All authors have given approval to the final version of the manuscript.

Conflicts of interest

There are no conflicts to declare.

Acknowledgements

References

1 K. Deng, Z. Luo, L. Tan and Z. Quan, Self-assembly of anisotropic nanoparticles into functional superstructures, *Chem. Soc. Rev.*, 2020, **49**, 6002–6038.

2 X. Li, X. Liu and X. Liu, Self-assembly of colloidal inorganic nanocrystals: nanoscale forces, emergent properties and applications, *Chem. Soc. Rev.*, 2021, **50**, 2074–2101.

3 S. Lee, K. Sim, S. Y. Moon, J. Choi, Y. Jeon, J.-M. Nam and S.-J. Park, Controlled assembly of plasmonic nanoparticles: from static to dynamic nanostructures, *Adv. Mater.*, 2021, **33**, 2007668.

4 F. Gambinossi, S. E. Mylon and J. K. Ferri, Aggregation kinetics and colloidal stability of functionalized nanoparticles, *Adv. Colloid Interface Sci.*, 2015, **222**, 332–349.

5 R. J. Hunter, *Foundations of Colloid Science*, Oxford University Press, 2001.

6 L. D. Pachón and G. Rothenberg, Transition-metal nanoparticles: synthesis, stability and the leaching issue, *Appl. Organomet. Chem.*, 2008, **22**, 288–299.

7 D. Segets, R. Marczak, S. Schäfer, C. Paula, J.-F. Gnichwitz, A. Hirsch and W. Peukert, Experimental and theoretical studies of the colloidal stability of nanoparticles – a general interpretation based on stability maps, *ACS Nano*, 2011, **5**, 4658–4669.

8 G. Garnweitner, H. Ghareeb and C. Grote, Small-molecule *in situ* stabilization of TiO$_2$ nanoparticles for the facile preparation of stable colloidal dispersions, *Colloids Surf., A*, 2010, **372**, 41–47.

9 R. A. Sperling and W. J. Parak, Surface modification, functionalization and bioconjugation of colloidal inorganic nanoparticles, *Philos. Trans. R. Soc., A*, 2010, **368**, 1333–1383.

10 J. P. Vanegas, J. C. Scaiano and A. E. Lanterna, Thiol-stabilized gold nanoparticles: new ways to displace thiol layers using yttrium or lanthanide chlorides, *Langmuir*, 2017, **33**, 12149–12154.

11 E. Pensa, E. Cortés, G. Corthey, P. Carro, C. Vericat, M. H. Fonticelli, G. Benítez, A. A. Rubert and R. C. Salvarezza, The chemistry of the sulfur–gold interface: in search of a unified model, *Acc. Chem. Res.*, 2012, **45**, 1183–1192.

12 P. Zhao, N. Li and D. Astruc, State of the art in gold nanoparticle synthesis, *Coord. Chem. Rev.*, 2013, **257**, 638–665.

13 A. Dorris, S. Rucareanu, L. Reven, C. J. Barrett and R. B. Lennox, Preparation and characterization of polyelectrolyte-coated gold nanoparticles, *Langmuir*, 2008, **24**, 2532–2538.

14 Q. K. Nguyen, T. H. Hoang, X. T. Bui, T. A. H. Nguyen, T. D. Pham, T. Pham and N. M. AuthorAnonymous, Synthesis and application of polycation-stabilized gold nanoparticles as a highly sensitive sensor for molecular cysteine determination, *Microchem. J.*, 2021, **168**, 106481.

15 J. R. Navarro, A. Liotta, A.-C. Faure, F. Lerouge, F. Chaput, G. Micouin, P. L. Baldeck and S. Parola, Tuning dye-to-particle interactions toward luminescent gold nanostars, *Langmuir*, 2013, **29**, 10915–10921.

16 S. T. Sivapalan, J. H. Vella, T. K. Yang, M. J. Dalton, R. N. Swiger, J. E. Ha-ley, T. M. Cooper, A. M. Urbas, L.-S. Tan and C. J. Murphy, Plasmonic en-hancement of the two photon absorption cross section of an organic chromophore using polyelectrolyte-coated gold nanorods, *Langmuir*, 2012, **28**, 9147–9154.

17 J. Najeeb, U. Farwa, F. Ishaque, H. Munir, A. Rahdar, M. F. Nazar and M. N. Zafar, Surfactant stabilized gold nanomaterials for environmental sensing applications – a review, *Environ. Res.*, 2022, **208**, 112644.

18 J. Turkevich, P. C. Stevenson and J. Hillier, A study of the nucleation and growth pro-cesses in the synthesis of colloidal gold, *Discuss. Faraday Soc.*, 1951, **11**, 55–75.

19 J. G. Mehtala, D. Y. Zemlyanov, J. P. Max, N. Kadasala, S. Zhao and A. Wei, Citrate-stabilized gold nanorods, *Langmuir*, 2014, **30**, 13727–13730.

20 H. Al-Johani, *et al.*, The structure and binding mode of citrate in the stabilization of gold nanoparticles, *Nat. Chem.*, 2017, **9**, 890–895.

21 G. González-Rubio, L. Scarabelli, A. Guerrero-Martínez and L. M. Liz-Marzán, Surfactant-assisted symmetry breaking in colloidal gold nanocrystal growth, *ChemNanoMat*, 2020, **6**, 698–707.

22 C. J. Johnson, E. Dujardin, S. A. Davis, C. J. Murphy and S. Mann, Growth and form of gold nanorods prepared by seed-mediated, surfactant-directed synthesis, *J. Mater. Chem.*, 2002, **12**, 1765–1770.

23 S. K. Meena, F. Lerouge, P. Baldeck, C. Andraud, M. Garavelli, S. Parola, M. Sulpizi and I. Rivalta, On the origin of controlled anisotropic growth of monodisperse gold nanobipyramids, *Nanoscale*, 2021, **13**, 15292–15300.

24 B. Nikoobakht and M. A. El-Sayed, Evidence for bilayer assembly of cationic surfactants on the surface of gold nanorods, *Langmuir*, 2001, **17**, 6368–6374.

25 T. K. Sau and C. J. Murphy, Self-assembly patterns formed upon solvent evaporation of aqueous cetyltrimethylammonium bromide-coated gold nanoparticles of various shapes, *Langmuir*, 2005, **21**, 2923–2929.

26 N. D. Burrows, W. Lin, J. G. Hinman, J. M. Dennison, A. M. Vartanian, N. S. Abadeer, E. M. Grzincic, L. M. Jacob, J. Li and C. J. Murphy, Surface chemistry of gold nanorods, *Langmuir*, 2016, **32**, 9905–9921.

27 S. Gómez-Graña, F. Hubert, F. Testard, A. Guerrero-Martínez, I. Grillo, L. M. Liz-Marzan and O. Spalla, Surfactant (Bi)layers on gold nanorods, *Langmuir*, 2012, **28**, 1453–1459.

28 F. Barbero, O. H. Moriones, N. G. Bastús and V. Puntes, Dynamic equilibrium in the cetyltrimethylammonium bromide–au nanoparticle bilayer, and the consequent impact on the formation of the nanoparticle protein corona, *Bioconjugate Chem.*, 2019, **30**, 2917–2930.

29 S. Lee, L. J. E. Anderson, C. M. Payne and J. H. Hafner, Structural transition in the surfactant layer that surrounds gold nanorods as observed by analytical surface-enhanced raman spectroscopy, *Langmuir*, 2011, **27**, 14748–14756.

30 C. A. Silvera Batista, R. G. Larson and N. A. Kotov, Nonadditivity of nanoparticle interactions, *Science*, 2015, **350**, 1242477.

31 B. Abécassis, Three-dimensional self assembly of semiconducting colloidal nanocrystals: from fundamental forces to collective optical properties, *ChemPhysChem*, 2016, **17**, 618–631, DOI: 10.1002/cphc.201500856.

32 D. Chateau, A. Desert, F. Lerouge, G. Landaburu, S. Santucci and S. Parola, Beyond the concentration limitation in the synthesis of nanobipyramids and other pentatwinned gold nanostructures, *ACS Appl. Mater. Interfaces*, 2019, **11**, 39068–39076.

33 D. Chateau, A. Liotta, F. Vadcard, J. R. G. Navarro, F. Chaput, J. Lermé, F. Lerouge and S. Parola, From gold nanobipyramids to nanojavelins for a precise tuning of the plasmon resonance to the infrared wavelengths:

experimental and theoretical aspects, *Nanoscale*, 2015, **7**, 1934–1943.

34 A. Carone, P. Mariani, A. Désert, M. Romanelli, J. Marcheselli, M. Garavelli, S. Corni, I. Rivalta and S. Parola, Insight on chirality encoding from small thiolated molecule to plasmonic Au@Ag and Au@Au nanoparticles, *ACS Nano*, 2022, **16**, 1089–1101.

35 Z. J. Hu, S. Hou, Y. L. Ji, T. Wen, W. Q. Liu, H. Zhang, X. W. Shi, J. Yan and X. C. Wu, Fast characterization of gold nanorods ensemble by correlating its structure with optical extinction spectral features, *AIP Adv.*, 2014, **4**, 117137.

36 L. Gunnarsson, T. Rindzevicius, J. Prikulis, B. Kasemo, M. Käll, S. Zou and G. C. Schatz, Confined plasmons in nanofabricated single silver particle pairs: experimental observations of strong interparticle interactions, *J. Phys. Chem. B*, 2005, **109**, 1079–1087.

37 B. Sepúlveda, P. C. Angelomé, L. M. Lechuga and L. M. Liz-Marzán, LSPR-based nanobiosensors, *Nano Today*, 2009, **4**, 244–251.

38 B. E. Janicek, J. G. Hinman, J. J. Hinman, S. H. Bae, M. Wu, J. Turner, H.-H. Chang, E. Park, R. Lawless, K. S. Suslick, C. J. Murphy and P. Y. Huang, Quantitative imaging of organic ligand density on anisotropic inorganic nanocrystals, *Nano Lett.*, 2019, **19**, 6308–6314.

39 L. Vigderman, B. P. Khanal and E. R. Zubarev, Functional gold nanorods: synthesis, self-assembly, and sensing applications, *Adv. Mater.*, 2012, **24**, 4811–4841.

40 M. Yang, G. Chen, Y. Zhao, G. Silber, Y. Wang, S. Xing, Y. Han and H. Chen, Mechanistic investigation into the spontaneous linear assembly of gold nanospheres, *Phys. Chem. Chem. Phys.*, 2010, **12**, 11850.

41 H. Zhang and D. Wang, Controlling the growth of charged-nanoparticle chains through interparticle electrostatic repulsion, *Angew. Chem., Int. Ed.*, 2008, **47**, 3984–3987.

42 A. Kar, M. Singh, D. Paital and S. Khatua, Establishing surface charge as a key control parameter for linker-driven tip-specific ordering of anisotropic gold nanoparticles, *J. Phys. Chem. C*, 2021, **125**, 23895–23903.

43 A. M. Funston, C. Novo, T. J. Davis and P. Mulvaney, Plasmon coupling of gold nanorods at short distances and in different geometries, *Nano Lett.*, 2009, **9**, 1651–1658.

44 X. Li, J. Lyu, C. Goldmann, M. Kociak, D. Constantin and C. Hamon, Plasmonic oligomers with tunable conductive nanojunctions, *J. Phys. Chem. Lett.*, 2019, **10**, 7093–7099.

45 A. A. Ensafi, B. Hemmateenejad and S. Barzegar, Non-extraction flow injection determi-nation of cationic surfactants using eriochrome black-T, *Spectrochim. Acta, Part A*, 2009, **73**, 794–798.